REPORT DOCUMENTATION PAGE

Form Approved OMB NO. 0704-0188

1. REPORT DATE (DD-MM-YYYY)	2. REPORT TYPE	3. DATES COVERED (From - To)
02-01-2011	Final Report	1-Sep-2006 - 31-Aug-2010

4. TITLE AND SUBTITLE

Microstructural Modeling and Representation of Simultaneous Failure Modes in Crystalline Aggregates Subjected to Dynamic Loading Conditions

5a. CONTRACT NUMBER
W911NF-06-1-0416

5b. GRANT NUMBER

5c. PROGRAM ELEMENT NUMBER
611102

6. AUTHORS
Zikry, M.A.

5d. PROJECT NUMBER

5e. TASK NUMBER

5f. WORK UNIT NUMBER

7. PERFORMING ORGANIZATION NAMES AND ADDRESSES

North Carolina State University
Office of Contract and Grants
Leazar Hall Lower Level- MC
Raleigh, NC 27695 -7214

8. PERFORMING ORGANIZATION REPORT NUMBER

9. SPONSORING/MONITORING AGENCY NAME(S) AND ADDRESS(ES)

U.S. Army Research Office
P.O. Box 12211
Research Triangle Park, NC 27709-2211

10. SPONSOR/MONITOR'S ACRONYM(S)
ARO

11. SPONSOR/MONITOR'S REPORT NUMBER(S)
51007-EG.1

12. DISTRIBUTION AVAILIBILITY STATEMENT

Approved for Public Release; Distribution Unlimited

13. SUPPLEMENTARY NOTES

The views, opinions and/or findings contained in this report are those of the author(s) and should not contrued as an official Department of the Army position, policy or decision, unless so designated by other documentation.

14. ABSTRACT

This provides an integrated framework to simultaneously handle different interrelated physical mechanisms, such as a myriad of representative dislocation-density interactions with high and low angle GB interfaces, the growth and coalescence of a population of voids, and how these interactions can lead to either intergranular or transgranular failure. The formation of pile-ups at GB interfaces, as a function of dislocation-density partial and total blockage and absorption at GB interfaces, will be determined and related to behavior at the grain and

15. SUBJECT TERMS

Failure, High Strain-Rate, Shear Strain Localization

16. SECURITY CLASSIFICATION OF:			17. LIMITATION OF ABSTRACT	15. NUMBER OF PAGES	19a. NAME OF RESPONSIBLE PERSON
a. REPORT	b. ABSTRACT	c. THIS PAGE			Mohammed Zikry
UU	UU	UU	UU		19b. TELEPHONE NUMBER: 919-515-5237

Report Title

Microstructural Modeling and Representation of Simultaneous Failure Modes in Crystalline Aggregates Subjected to Dynamic Loading Conditions

ABSTRACT

This provides an integrated framework to simultaneously handle different interrelated physical mechanisms, such as a myriad of representative dislocation-density interactions with high and low angle GB interfaces, the growth and coalescence of a population of voids, and how these interactions can lead to either intergranular or transgranular failure. The formation of pile-ups at GB interfaces, as a function of dislocation-density partial and total blockage and absorption at GB interfaces, will be determined and related to behavior at the grain and aggregate levels. How pile-ups form, and whether stress fields accumulate or are relaxed by GB distributions and orientations, GB morphology, and local cohesive strengths, will be determined and related to void nucleation, growth, and coalescence.

List of papers submitted or published that acknowledge ARO support during this reporting period. List the papers, including journal references, in the following categories:

(a) Papers published in peer-reviewed journals (N/A for none)

1. J. Shi and M.A. Zikry (2009), Grain-boundary interactions and orientation effects on crack behavior in polycrystalline aggregates, International Journal Of Solids And Structures 46, 341-369.

2. J. Shi and M.A. Zikry (2009), Grain size, grain boundary sliding, and grain boundary interaction effects on nanocrystalline behavior, Materials Science and Engineering A 520, 121-133.

3. F. Jawad and M. A. Zikry (2009), The Effects of Grain-Boundary Orientations on Failure Behavior in F.C.C. Polycrystalline Systems, International Journal of Damage Mechanics 18, 341-369.

4. O. Rezvanian and M.A. Zikry (2008), Microstructure Characterization And Modeling In F.C.C Crystalline Materials In a Unified Dislocation Density Framework, Materials Science and Engineering A 494, pp. 80-85.

5. O. Rezvanian and M.A. Zikry (2007), Statistically Stored, Geometrically Necessary and Grain Boundary Dislocation Densities: Microstructural Representation and Modelling, Philosophical Transactions Of The Royal Society of London. Series A, Mathematical, Physical and Engineering Sciences, 463/ 2087, 2833-2853

6.O. Rezvanian and M.A. Zikry (2007), Microstructural Modeling of Grain Subdivision and Large Strain Inhomogeneous Deformation Modes in F.C.C. Crystalline Materials in Size Effects in the Deformation of Materials — Experiments and Modeling, edited by E. Lilleodden, P. Besser, L. Levine, A. Needleman (Mater. Res. Soc. Symp. Proc. 976E, Warrendale, PA, 2007), EE2.02

7. O. Rezvanian, M.A. Zikry, and A.M. Rajendran (2006), Microstructural Modeling of Grain Subdivision and Large Strain Inhomogeneous Deformation Modes in F.C.C. Crystalline Materials, Mechanics of Materials 38, 1159-1169

8.J. Shi, M.A. Zikry and T. Hatem (2007), Modeling of Grain-Boundary Ledges, in Multiscale Modeling of Materials, edited by R. Devanathan, M. J. Caturla, A. Kubota, A. Chartier, S. Phillpot (Mater. Res. Soc. Symp. Proc. 978E, Warrendale, PA, 2007), pp. G3.9-3.7

Number of Papers published in peer-reviewed journals: 8.00

(b) Papers published in non-peer-reviewed journals or in conference proceedings (N/A for none)

1. J. Shi, T. Hatem, M.A. Zikry (2008), Failure modes and Grain-Boundary Effects, Proceedings of The Second International Conference on Advances in Heterogeneous Material Mechanics (ICHMM-2008), Ed: J. Fan and H. Chen, pp. 62-68.

2. O. Rezvanian and M.A. Zikry (2008), Failure Modes in F.C.C. Crystalline Materials in Plasticity, Failure, and Fatigue in Structural Materials from Macro to Nano: Proceedings of the Hael Mughrabi Honorary Symposium, TMS (The Metals Society), eds.: Jimmy Hsia, Mathias Goken, Tresa Pollock, Pedro Portella, and Neville Mood, pp. 61-69.

3. O. Rezvanian and M.A. Zikry (2007), Microstructural Modeling of Grain Subdivision and Large Strain Inhomogeneous Deformation Modes in F.C.C. Crystalline Materials in Advances in Microstructure-Based Modeling and Characterization of Deformation Microstructures, TMS (The Metals Society), eds.: R. Shalabian, S. Agnew, pp. 23-29

Number of Papers published in non peer-reviewed journals: 3.00

(c) Presentations

• Microstructural Modeling of Failure Modes in Crystalline Materials, X International Conference on Computational Plasticity, Barcelona, Spain, 2009.
• Microstructural Modeling of Failure Modes in Crystalline Materials, 12th International Conference on Fracture, Ottawa, Canada, 2009.
• Microstructural Effects and Dislocation Density Evolution in Crystalline Aggregates, World Symposium On Multiscale Material Mechanics And Engineering Sciences: In Memory of Frank Nabarro, Edward Hart, Ronald Rivlin, Thessaloniki, Greece, April, 2007
• Microstructural Modeling of Grain Subdivision, presented at The Metals Society Annual Meeting, Orlando, FL, February, 2007
• Modeling of GB Ledges, presented at the Materials Research Society Annual Meeting, Boston, MA, December, 2006

Number of Presentations: 5.00

Non Peer-Reviewed Conference Proceeding publications (other than abstracts):

Number of Non Peer-Reviewed Conference Proceeding publications (other than abstracts): 0

Peer-Reviewed Conference Proceeding publications (other than abstracts):

Number of Peer-Reviewed Conference Proceeding publications (other than abstracts): 0

(d) Manuscripts

Number of Manuscripts: 0.00

Patents Submitted

Patents Awarded

Awards

• Distinguished Research Award, NCSU, 2010
• Outstanding Paper, Symposium HH Materials Research Society, 2009
• Jefferson Science Fellow, U.S. State Department, 2008-Present
• Research Excellence Award, NCSU, 2008
• ALCOA Senior Distinguished Research Award, 2007

Graduate Students

NAME	PERCENT_SUPPORTED
J. Shi	0.50
FTE Equivalent:	**0.50**
Total Number:	**1**

Names of Post Doctorates

NAME	PERCENT_SUPPORTED
O. Rezvanian	0.20
FTE Equivalent:	**0.20**
Total Number:	**1**

Names of Faculty Supported

NAME	PERCENT_SUPPORTED	National Academy Member
M.A. Zikry	0.20	No
FTE Equivalent:	**0.20**	
Total Number:	**1**	

Names of Under Graduate students supported

NAME	PERCENT_SUPPORTED
FTE Equivalent:	
Total Number:	

Student Metrics

This section only applies to graduating undergraduates supported by this agreement in this reporting period

The number of undergraduates funded by this agreement who graduated during this period:	0.00
The number of undergraduates funded by this agreement who graduated during this period with a degree in science, mathematics, engineering, or technology fields:.....	0.00
The number of undergraduates funded by your agreement who graduated during this period and will continue to pursue a graduate or Ph.D. degree in science, mathematics, engineering, or technology fields:.....	0.00
Number of graduating undergraduates who achieved a 3.5 GPA to 4.0 (4.0 max scale):	0.00
Number of graduating undergraduates funded by a DoD funded Center of Excellence grant for Education, Research and Engineering:	0.00
The number of undergraduates funded by your agreement who graduated during this period and intend to work for the Department of Defense	0.00
The number of undergraduates funded by your agreement who graduated during this period and will receive scholarships or fellowships for further studies in science, mathematics, engineering or technology fields:	0.00

Names of Personnel receiving masters degrees

NAME
Total Number:

Names of personnel receiving PHDs

NAME
J. Shi
T. Hatem
Total Number: 2

Names of other research staff

NAME	PERCENT_SUPPORTED
FTE Equivalent:	
Total Number:	

Sub Contractors (DD882)

Inventions (DD882)

PHILOSOPHICAL MAGAZINE, 1 Nov–1 Dec 2003
VOL. 83, NOS. 31–34, 3917–3944

Taylor & Francis
Taylor & Francis Group

Grain-boundary interfaces and void interactions in porous aggregates

W. M. ASHMAWI and M. A. ZIKRY†

Department of Mechanical and Aerospace Engineering, North Carolina State University, Raleigh, North Carolina 27695-7910, USA

[*Received 10 November 2002 and in final form 17 March 2003*]

ABSTRACT

A multiple-slip dislocation-density-based formulation and computational schemes that are coupled to grain-boundary (GB) interfacial schemes and an internal porosity formulation are used to analyse the behaviour and interaction of different arrangements and geometries of explicit pairs of voids in a polycrystalline fcc aggregate. The GB regions are treated as regions with properties and topologies that are distinct from that of the grain bulk. The GB kinematic scheme accounts for dislocation density interactions with GBs, such as dislocation density impedance, blockage and GB absorption. These evolving interfacial conditions are monitored throughout the deformation history. The analysis indicated that void-to-void interactions result in dislocation density evolution and saturation and porosity localization that are intricately related to both dislocation density pile-ups and blockages at GB interfaces, and GB absorption within different GB regions.

§1. INTRODUCTION

GB structure and orientation are crucial factors in the characterization of ductile and brittle failure modes in polycrystalline materials. These GBs, generally consisting of transition regions of highly distorted crystalline structure between mis-oriented grains, with material properties that are generally distinct from those of bulk grains, can accelerate, retard or inhibit the initiation and the evolution of failure modes. As noted by Schmitz *et al*. (1989) and Davies and Randle (2001), the early stages of material failure in crystalline materials are not characterized by crack nucleation in individual grains, but the critical first step is the propagation of the crack *across or along* a GB plane. The dislocation characteristics, the interface and grain properties, the topological effects of internal microstructure, and the cohesive strength of evolving internal GB properties are intricately related to failure initiation and evolution.

The *physical scale* on which GB effects are investigated has a direct bearing on understanding and accurately predicting the material mechanisms that trigger failure. On a macroscopic spatial scale, it is generally assumed in most analyses of polycrystalline deformations that the grains are homogeneous, and that the GBs

†Email: zikry@eos.ncsu.edu.

Philosophical Magazine ISSN 1478–6435 print/ISSN 1478–6443 online
http://www.tandf.co.uk/journals
DOI: 10.1080/14786430310001599423

are only locations where stress equilibrium and strain boundary conditions have to be satisfied. The presence of GBs, on this scale, results in the redistribution of stresses due to compatibility requirements for elastic and inelastic deformations. However, since crystalline grains are generally anisotropic, the deformations due to external stresses are not generally compatible, and therefore additional stresses must be induced to match the shape of a strained grain with neighbouring grains. Furthermore, when the grains are plastically deformed by inelastic slip on specific crystallographic slip systems, the deformations for different orientations are not compatible and additional stresses may also arise. Plastic slip is also generally inhomogeneous, since it is spatially localized; this can further redistribute the stresses at the GB (for example Kroner (1986)). On a microscopic scale, lattice dislocations interact with the GB, which acts as an obstacle to their motion. The strength of these obstacles depends on the interaction of the GBs with the dislocations. The dislocations impinging on the GB can increase the magnitude of the stress field in the adjoining grains and may promote nucleation of lattice dislocations in the grain. When dislocations penetrate from one grain to the next, residual dislocations may be left behind in the boundary. Therefore, the strength of the obstacle may depend on the Burgers vector of residual boundary dislocations that are created by penetrating lattice dislocations (Gleiter 1982).

Furthermore, experimental results (for example Lee *et al*. (1990) and Marguiles *et al*. (2001)) have clearly indicated how slip transmits through GBs and how, if the slip is impeded, cracks can nucleate along the GB plane, resulting in intergranular fracture. The significance of these results is that, owing to plastic deformation, dislocations pile up against an interface, and then cracks nucleate and grow along the GB. Therefore, it is essential not only to deal with a density of dislocations for large inelastic deformations in aggregates with different GB interfaces but also to treat GBs as interfacial planes with properties distinct from those of the bulk, where a population of dislocations from different adjacent grains are absorbed or nucleated.

One of the current challenges is how to account for different dislocation density interactions with GB interfaces with distinct topologies and properties, and how these interactions affect ductile failure nucleation and growth on different physical scales. Interfacial misorientations between grains due to the translation and rotation of one crystalline lattice with respect to adjacent grains in combination with the other defects such as cracks and voids can result in the formation of dislocation density pile-ups at GB interfaces, or the absorption of dislocation densities within the GB region, or the partial transmission of dislocation densities across GB interfaces to neighbouring grains (Watanabe 1989, Baker and Liu 1994). Numerous investigations have clearly indicated that intrinsic thermomechanical properties, operative crystallographic systems and dislocation mechanisms associated with GB regions all may be substantially different from those associated with the aggregate crystalline bulk response (Dingley and Pond 1979, Baker and Liu 1994, Randle 1997, Davies and Randle 2001). However, the effects of how these GB interactions and mechanisms, such as slip transmission, impedance and blockage, affect void nucleation and growth on different physical scales are not well understood and have not been adequately quantified (Watanabe and Tsurekawa 1999).

The major objective of this study is to understand how dislocation density interactions with GB interfaces affect microvoid nucleation and growth, and how

this is related to material behaviour and interactions with different explicit pairs of void distributions and arrangements at the local and global levels. A kinematically based scheme that is coupled to a dislocation density multiple-slip formulation (Ashmawi and Zikry 2002) is used to account for the interactions of dislocation densities with GB interfaces in polycrystalline aggregates. This methodology is used with an internal porosity formulation that accounts for microvoid growth and nucleation. In this study, the microvoid nucleation internal variable is a function of updated values of the total dislocation density, stress triaxiality, accumulated plastic strains and temperature. GB interfaces are treated as regions with distinct width properties and topologies. Schemes are then introduced to monitor how dislocation density evolutions on different operative slip systems interact with GB interfaces, and how dislocation density evolution can result in slip transmission, impedance and blockage. Furthermore, it is shown how this can result in dislocation density pile-ups at GB interfaces, or dislocation density absorption within the GB region, or dislocation density transmission to neighbouring grains.

This paper is organized as follows: the dislocation-density-based multiple-slip crystalline formulation is introduced in § 2; the dislocation density evolution is presented in § 3; the kinematic scheme for the interaction of dislocation densities and slip with GB interfaces is outlined in § 4; the internal porosity formulation is introduced in § 5; the computational method is given in § 6; the results are presented and discussed in § 7; the summary and conclusions are given in § 8.

§ 2. Dislocation density-based multiple-slip constitutive formulation

The formulation for the multiple-slip crystal plasticity rate-dependent constitutive relations, and the derivation of the evolutionary equations for the mobile and immobile dislocation densities, which are coupled to the multiple-slip crystalline formulation, are presented. The formulation is based on that developed by Zikry and Kao (1996) and Ashmawi and Zikry (2000, 2003).

It is assumed that the velocity gradient can be decomposed into a symmetric part, the deformation rate tensor D_{ij} and an antisymmetric part, the spin tensor W_{ij}. It is further assumed that the total deformation rate tensor D_{ij} and the total spin tensor W_{ij} can be then additively decomposed into elastic and plastic components:

$$D_{ij} = D^{*}_{ij} + D^{\mathrm{p}}_{ij}, \tag{1a}$$

$$W_{ij} = W^{*}_{ij} + W^{\mathrm{p}}_{ij}, \tag{1b}$$

in which W_{ij} includes the rigid-body spin. The inelastic parts are defined in terms of the crystallographic slip rates as

$$D^{\mathrm{p}}_{ij} = P^{(\alpha)}_{ij}\dot{\gamma}^{(\alpha)}, \tag{2a}$$

$$W^{\mathrm{p}}_{ij} = \omega^{(\alpha)}_{ij}\dot{\gamma}^{(\alpha)}, \tag{2b}$$

where α is summed over all slip systems, and $P^{(\alpha)}_{ij}$ and $\omega^{(\alpha)}_{ij}$ are second-order tensors, defined in terms of the unit normals to the slip planes and the unit slip vectors to the slip directions.

For rate-dependent inelastic materials, the constitutive description on each slip system can be characterized by a power-law relation

$$\dot{\gamma}^{(\alpha)} = \dot{\gamma}^{(\alpha)}_{\mathrm{ref}} \frac{\tau^{(\alpha)}}{\tau^{(\alpha)}_{\mathrm{ref}}} \left(\frac{\left|\tau^{(\alpha)}\right|}{\tau^{(\alpha)}_{\mathrm{ref}}} \right)^{1/m-1}, \quad \text{no sum on } \alpha, \tag{3}$$

where $\dot{\gamma}^{(\alpha)}_{\mathrm{ref}}$ is the reference shear strain rate which corresponds to a reference shear stress $\tau^{(\alpha)}_{\mathrm{ref}}$ and m is the rate sensitivity parameter. The reference stress that is used here is a modification of widely used classical forms (Mughrabi 1987) that relate the reference stress to a square root dependence on the dislocation density as

$$\tau^{(\alpha)}_{\mathrm{ref}} = \tau^{(\alpha)}_{\mathrm{y}} + Gb \sum_{\xi=1}^{12} a_{\xi} \left(\rho^{(\xi)}_{\mathrm{im}} \right)^{1/2}, \tag{4}$$

where G is the shear modulus, b is the magnitude of the Burgers vector, $\tau^{(\alpha)}_{\mathrm{y}}$ is the static yield stress and the coefficients a_{ξ} are interaction coefficients that generally have a magnitude of unity.

§ 3. The evolutions of mobile and immobile dislocation densities

At a given state for a deformed material, the dislocation structure of total dislocation density $\rho^{(\alpha)}$ can be assumed to be additively decomposed into a mobile dislocation density $\rho^{(\alpha)}_{\mathrm{m}}$ and an immobile dislocation density $\rho^{(\alpha)}_{\mathrm{im}}$:

$$\rho^{(\alpha)} = \rho^{(\alpha)}_{\mathrm{m}} + \rho^{(\alpha)}_{\mathrm{im}}. \tag{5}$$

It is assumed that, during an increment of strain, an immobile dislocation density rate is generated and an immobile dislocation density rate is annihilated for statistically stored dislocation densities (for example Liu *et al.* (1998)). The balance between dislocation generation and annihilation equations is the basis for the evolution of mobile and immobile dislocation densities as a function of strain. Based on these arguments, it can be shown (see the paper by Kameda and Zikry (1996) for a detailed presentation) that the coupled set of nonlinear evolutionary equations of mobile and immobile dislocation densities can then be given by

$$\frac{\mathrm{d}\rho^{(\alpha)}_{\mathrm{m}}}{\mathrm{d}t} = \dot{\gamma}^{(\alpha)} \left[\frac{g_{\mathrm{sour}}}{b^2} \frac{\rho^{(\alpha)}_{\mathrm{im}}}{\rho^{(\alpha)}_{m}} - \frac{g_{\mathrm{minter}}}{b^2} \exp\left(-\frac{H}{kT} \right) - \frac{g_{\mathrm{immob}}}{b} \left(\rho^{(\alpha)}_{\mathrm{im}} \right)^{1/2} \right], \tag{6}$$

$$\frac{d\rho^{(\alpha)}_{\mathrm{im}}}{\mathrm{d}t} = \dot{\gamma}^{(\alpha)} \left[\frac{g_{\mathrm{minter}}}{b^2} \exp\left(-\frac{H}{kT} \right) + \frac{g_{\mathrm{immob}}}{b} \left(\rho^{(\alpha)}_{\mathrm{im}} \right)^{1/2} - g_{\mathrm{recov}} \exp\left(-\frac{H}{kT} \right) \rho^{(\alpha)}_{\mathrm{im}} \right], \tag{7}$$

where g_{sour} is a coefficient pertaining to an increase in the mobile dislocation density due to dislocation sources, g_{minter} is a coefficient related to the trapping of mobile dislocations due to forest intersections, cross-slip around obstacles or dislocation interactions, g_{recov} is a coefficient related to the rearrangement and annihilation of immobile dislocations, g_{immob} is a coefficient related to the immobilization of mobile dislocations, H is the activation enthalpy and k is Boltzmann's constant. As these evolutionary equations indicate, the dislocation activities related to recovery and trapping are coupled to thermal activation.

To couple the evolutionary equations to the multiple-slip crystal plasticity formulation, the four g coefficients in equations (6) and (7) and the enthalpy H must be determined as functions of the deformation mode. The enthalpy H is

determined by defining an exponential ratio of the current temperature to the reference temperature. The four g coefficients are determined by using the following two general conditions pertinent to the evolution of dislocation densities in crystalline materials: that the mobile and immobile densities saturate at large strains, and that the relaxation of the mobile dislocation density to a quasisteady-state value occurs much more rapidly than the variation in the immobile density (Mughrabi 1987, Hansen 1990, Bay *et al*. 1992).

§ 4. Kinematics of dislocation density interactions with grain boundaries

As stated earlier, GBs can act as effective barriers to motion of lattice dislocations. Dislocation densities can accumulate within GB regions, and this accumulation within GB interfacial regions can lead to substantial increases in GB internal stresses and GB misorientations. As GB misorientations approach large angle values, GBs act as barriers to crystalline slip in the lattice, which can result in the formation of pile-ups that subsequently has a direct consequence on failure initiation and evolution.

There is a myriad of dislocation density interactions with GB interfaces, such as GB absorption of lattice dislocations without dissociation into grain-boundary dislocations (GBDs) (Baker *et al*. 1987, Baker and Liu 1994), partial dislocation transmission from one grain to the adjacent grain with a residual GBD left in the GB region (Lee *et al*. 1992, Baker and Liu 1994), full dislocation transmission from one grain to the adjacent grain with no residual GBD left in the GB region (Shen *et al*. 1988, Lee *et al*. 1992, Baker and Liu 1994), and dislocation absorption and subsequent re-emission from the GB (Shen *et al*. 1988).

In this study, we have focused on investigating the following representative interactions:

(i) full and partial dislocation density transmission from one grain to neighbouring grains;
(ii) full and partial dislocation density transmission into a GB and blockage at neighbouring grains;
(iii) dislocation density impedance and potential pile-ups.

These kinematic scenarios provide a general methodology that can be used as a framework for physically representative GB interfacial mechanisms and interactions.

A detailed presentation of the kinematic scheme for dislocation density transmission and impedance from one grain to neighbouring grains across GB regions has been given by Ashmawi and Zikry (2002). Only a brief outline will be given in this paper. The following steps are applied to determine the transmission, impedance, and absorption of dislocation densities at each GB interface in the aggregate.

(i) A potential dislocation density envelope is used to identify regions of high dislocation density activity (figure 1) on each corresponding slip system in regions adjacent to all GB interfaces. This dislocation density envelope encompasses all the finite elements immediately adjacent to the GB and that extend to the centre of each grain.
(ii) Coordinate frame transformations are performed with respect to each adjacent GB interface to identify the direction of the slip system orientation.

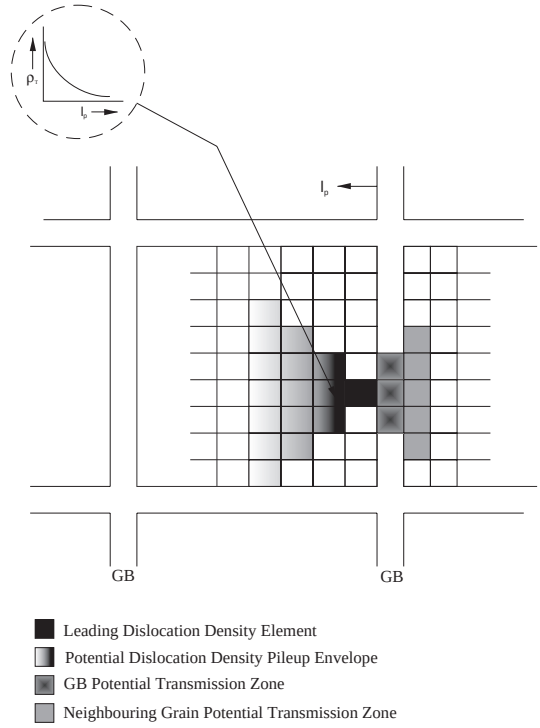

Figure 1. Dislocation density envelopes; l_p is the radial pile-up length.

(iii) Geometric compatibility conditions are then obtained to determine whether neighbouring slip systems are oriented for transmission or impedance through the GB.
(iv) If transmission is then possible through the GB, a transformation factor is calculated to provide a measure of how much of the dislocation density penetrates through the GB and into neighbouring grains.

4.1. *Potential dislocation density envelope*

It is essential to determine how dislocation densities evolve and accumulate near GB regions and what the maximum values and corresponding active slip system directions and orientations are, such that slip system impedance and transmission can be controlled and monitored in polycrystalline aggregates. Slip impedance at a GB can lead to pile-ups and stress accumulation, if neighbouring slip systems within the GB and adjacent grains are not activated and oriented for slip transmission. Therefore, it is crucial to identify the critical regions of dislocation density accumulation. A potential dislocation density envelope is used to identify these critical regions, and it is determined as follows.

(i) The maximum dislocation density on the corresponding slip system is identified in the region adjacent to the GB by monitoring the slip rate and dislocation density activity on each slip system.
(ii) This process is repeated until half of each grain diameter is transversed.

From this information, the envelope is constructed as shown in figure 1. This radial distribution is not constrained to be of any predetermined mathematical form. What this information provides is a distribution of the total dislocation density as a function of length orientation. This length l_p is a radial line that emanates from the GB to the middle of the grain. This radial line encompasses the dislocation density envelope. This potential dislocation density envelope can now be used to identify regions, in all eight adjacent grains, of potential transmission, or impedance, or blockage.

4.2. *Dislocation density orientation, grain-boundary coordinate frame transformation and slip plane geometric compatibility*

To ascertain how dislocation densities evolve near GB interfaces, it is essential to determine whether dislocation densities are moving away or towards the GBs. Hence, the orientation and direction of slip with respect to the GB will have to be determined. The GB normal vector $\tilde{\mathbf{n}}_{gb}$ and the in-plane vector $\tilde{\mathbf{m}}_{gb}$ are used to determine dislocation density directions and orientations. These coordinate transformations have to be performed for all slip systems on all *eight* GB interfaces for each grain.

Dislocation density transmission or impedance across GB interfacial regions are dependent not only on whether there are adjacent active slip systems but also on whether these slip systems are geometrically compatible, such that dislocation density transmission is possible across different slip systems. In this analysis, geometric compatibility will be defined by two angles θ and β (figure 2). If these values are exceeded, then transmission through the GB is *not* possible. The angle

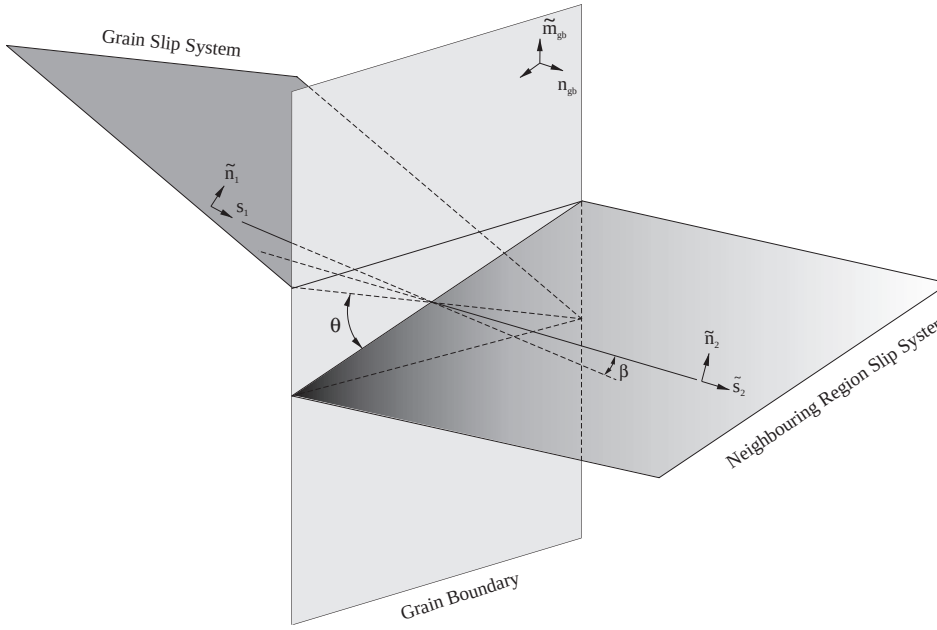

Figure 2. General slip plane geometric compatibility.

between the two intersection lines (vectors, $\tilde{\mathbf{l}}_1$ and $\tilde{\mathbf{l}}_2$) that represent the lines formed by the intersection of slip planes and the GB interfacial layer is given by

$$\cos\theta' = \frac{\tilde{\mathbf{l}}_1 \cdot \tilde{\mathbf{l}}_2}{|\tilde{\mathbf{l}}_1|\ |\tilde{\mathbf{l}}_2|}, \tag{8}$$

and θ is determined on the basis of the following two conditions:

$$\theta = \begin{cases} |\theta'| \\ \\ \pi - |\theta'| \end{cases} \quad \text{if} \quad \begin{cases} \theta' < \dfrac{\pi}{2}, \\ \\ \theta' > \dfrac{\pi}{2}. \end{cases} \tag{9}$$

Geometrically, it is clear that slip transmission is a maximum when $\theta = 0^\circ$. In this case, full transmission would occur. However, as noted by Werner and Prantl (1990) and Davies and Randle (2001), as θ increases, dislocation density transmission will be impeded. Also, slip planes intersecting the boundary generally maintain an angle of 15° or less (Werner and Prantl 1990). The second condition for ensuring geometric compatibility is therefore to monitor both slip plane orientations along the interfacial region with respect to an axis normal to a plane that includes GB normals and in-plane vectors. An angle β for this geometric compatibility can be determined by defining the dot product of two normals $\tilde{\mathbf{n}}_1$ and $\tilde{\mathbf{n}}_2$ to the slip planes on either side of the GB plane as

$$\cos\beta = \tilde{\mathbf{n}}_1 \cdot \tilde{\mathbf{n}}_2. \tag{10}$$

Full transmission (with respect to β compatibility) of slip takes place when $\beta = 0$. As a kink starts to form, for increasing value of $\theta = 0^\circ$, dislocation densities will be impeded. We shall assume that β compatibility is bounded by a value of 35°. As noted by Werner and Prantl (1990), these critical values of slip orientation are based on experimentally observed range of values for slip compatibility. In summary, dislocation densities can transmit when conditions of both θ compatibility and β compatibility are satisfied in conjunction with the other kinematic conditions outlined in this section.

4.3. *Transmission distribution factor*

Geometric slip system compatibility affects to a larger degree dislocation density transmission. The most favourable configuration occurs when $\theta = 0^\circ$ and $\beta = 0^\circ$, which indicates complete transmission. Deviation from this configuration would represent a partial transmission through the interface. A transmission factor ζ, based on θ and β, will be defined as

$$\zeta = \cos\theta\ \cos\beta. \tag{11}$$

This will provide a measure of how much of the dislocation density penetrates through the GB and into neighbouring grains. All activities on all slip systems have to be continually monitored on all eight GB regions for each grain in the aggregate. In some cases, pile-ups can be relieved by slip system rotations in neighbouring grains, or pile-ups may intensify as the deformation and failure modes *evolve*. In other cases, dislocation density transmission through the GB may occur by partial transmission on different slip systems into neighbouring grains. All these situations need to be delineated for accurate predictions of the effects of GB interfacial regions on overall behaviour.

§ 5. Internal void porosity evolution

As noted earlier, interrelated physical mechanisms can result in void nucleation, growth and coalescence. In this section, an internal porosity evolution is introduced. This evolution relation will be based on an internal variable f, which will account for microvoid nucleation and growth. This internal porosity relation will be coupled with the proposed dislocation-density-based crystalline constitutive formulation and the interfacial GB dislocation density interaction kinematic models to obtain predictions of void nucleation, growth and coalescence in polycrystalline aggregates. This will provide an understanding of how dislocation density evolution and GB interfaces affect microvoid nucleation and growth and how this is related to interactions with discrete void distributions. This will provide failure scenarios that can be used to determine how explicit voids interact with GB and dislocation density activities.

Void failure modelling will encompass two concurrent approaches. One approach will be based on the internal microvoid variable f, which will be coupled to the proposed methodologies, and the second approach will be based on modelling distributions of explicit voids with different geometries and morphologies within the aggregate.

Interrelated physical mechanisms can result in void nucleation, growth and coalescence. The internal porosity evolution relation is based on an internal variable, which accounts for microvoid nucleation and growth. It is assumed that the porosity evolution is due to microvoid growth and nucleation:

$$\dot{f} = \dot{f}_{\text{growth}} + \dot{f}_{\text{nucleation}}. \tag{12}$$

The rate $\dot{f}_{\text{growth}}$, of the growth of existing microvoid volume fraction is assumed to be due to matrix incompressibility:

$$\dot{f}_{\text{growth}} = (1-f)D^{\text{p}}_{kk}, \tag{13}$$

where D^{p}_{kk} is the trace of the inelastic part of the deformation rate tensor.

We assume that microvoid nucleation is a function of stress triaxiality, plastic slip accumulation, temperature (Garrison and Moody 1987, Magnusen *et al*. 1988, Needleman 1989, Becker and Smelser 1994) and dislocation density activities (Garrison and Moody 1987). Based on the discussion given in § 4 and detailed in the paper by Ashmawi and Zikry (2002), these dislocation density activities can encompass mechanisms such as slip incompatibilities and intersections that can lead to stress accumulation and pile-ups. It will be assumed that these variables have bounded nucleation rates as follows:

$$\frac{\rho_{\text{t}}^{(\beta)}}{\bar{\rho}_{\text{tsat}}} \rightarrow l_1, \tag{14a}$$

$$\frac{\sigma_{\text{m}}}{\sigma_{\text{y}}} \rightarrow l_2, \tag{14b}$$

$$\gamma \rightarrow l_3, \tag{14c}$$

$$\frac{T}{T_{\text{ref}}} \rightarrow l_4, \tag{14d}$$

where $\rho_t^{(\beta)}$ is the total dislocation density for the most active slip system β, $\bar{\rho}_{tsat}$ is the total saturated dislocation density, σ_m is the mean normal stress ($\sigma_{ii}/3$), σ_y is the static yield stress, γ is the accumulated plastic shear strain, T is the current temperature and T_{ref} is the reference temperature. These variables will be combined as

$$A = \frac{1}{l_1 l_2 l_3 l_4}. \tag{15}$$

Since nucleation is a continuous random process, the evolution formulation is assumed to be a statistical function of these pertinent parameters. Therefore, the microvoid nucleation rate can be postulated to evolve as

$$\dot{f}_{nucleation} = \aleph(\Psi; a, b)\Psi\left(\sigma_m, \rho_t^{(\beta)}, T, \gamma\right)\dot{f}_{nl}, \tag{16}$$

where $\dot{f}_{nl}$ is a nucleation rate limit, and the random variable Ψ will be given by

$$\Psi = A\,\frac{\rho_t^{(\beta)}}{\bar{\rho}_{tsat}}\,\frac{\sigma_m}{\sigma_y}\,\frac{T}{T_{ref}}\,\gamma, \tag{17}$$

such that $0 \leqslant \Psi \leqslant 1$, where Ψ is a field variable that represents a mapping of the interrelated local microstructural quantities that affect microvoid nucleation and growth. Since the internal porosity is generally random, it will be assumed that Ψ is a continuous random variable with gamma distribution, such that the distribution of Ψ can be represented with a probability distribution function of

$$\aleph(\Psi; a, b) = \frac{1}{b^a \Gamma(a)}\,\Psi^{a-1}\,\exp\left(-\frac{\Psi}{b}\right), \tag{18}$$

where $\Gamma(a)$ is the gamma function of a. The parameters a and b have positive values.

The nucleation rate limit $\dot{f}_{nl}$ is defined to be an upper material limit to microvoid nucleation

$$\dot{f}_{nl} = (f_{cr} - f)\frac{1}{dt}. \tag{19}$$

where f_{cr} is the maximum porosity for a material, f is the updated porosity and dt is the incremental time step.

The updated porosity is coupled with the flow stress associated with each slip system α as

$$\tilde{\tau}_{ref}^{(\alpha)} = \tau_{ref}^{(\alpha)}(1 - f), \tag{20}$$

where $\tilde{\tau}_{ref}^{(\alpha)}$ is the effective reference shear stress. Parametric studies were performed to assess the effects of varying these parameters and the initial porosity together with the variables a and b. Limiting values for each of the variables are given in table 1.

§ 6. Computational techniques

The total deformation rate tensor D_{ij} and the plastic deformation rate tensor D_{ij}^p are needed to update the material stress state. The method used here is one developed by Zikry (1994a) for rate-dependent crystalline plasticity formulations. An implicit finite-element method is used to obtain the total deformation rate tensor D_{ij}. To overcome numerical instabilities associated with stiffness, a hybrid explicit-implicit method is used to obtain the plastic deformation rate tensor D_{ij}^p. This hybrid

Table 1. Porosity parameters.

Parameter	Value
σ_m/σ_y	3.0
$\rho_t/\bar{\rho}_{tsat}$	0.95
T/T_{ref}	2.0
γ	1.0
a	2
b	1
f_{cr}	0.17

Table 2. Properties of grains and GB interfacial regions.

	Grain bulk	GB interfacial region
Young's modulus E	110 GPa	110 GPa
Static yield stress σ_y	110 MPa	330 MPa
Poisson's ratio ν	0.30	0.30
Rate sensitivity parameter m	0.005	0.005
Reference strain rate $\dot{\gamma}_{ref}$	$0.001\,s^{-1}$	$0.001\,s^{-1}$
Critical strain rate $\dot{\gamma}_{critical}$	$10^4\,s^{-1}$	$10^4\,s^{-1}$
Burgers vector b	3.0×10^{-10} m	3.0×10^{-10} m
Reference stress interaction coefficients a_i ($i=1$, 12)	0.50	0.50
Initial immobile dislocation density $\rho_{im}^{(\alpha)}$	$10^{10}\,m^{-2}$	Varies as a function of GB orientation, 10^{10}–$10^{12}\,m^{-2}$
Initial mobile dislocation density $\rho_{m}^{(\alpha)}$	$10^{7}\,m^{-2}$	Varies as a function of GB orientation, 10^{5}–$10^{7}\,m^{-2}$

numerical scheme is also used to update the evolutionary equations for the mobile and immobile densities.

§ 7. Results and discussion

The multiple-slip dislocation-density-based crystal plasticity formulation, the specialized finite-element algorithm, the GB interfacial interaction scheme and the internal porosity formulation were applied to investigate the effects of the interactions of multiple-slip systems and mobile and immobile dislocation densities with GB regions to determine how slip transmission, impedance, blockage and absorption affect microvoid nucleation and growth in a polycrystalline aggregate with explicit void pairs. The material properties (table 2) that are used here are representative of polycrystalline copper (Zikry 1994b). A random-number generator developed by Ashmawi and Zikry (2000) was used to misorient the grains and GB regions by the use of the three Euler angles φ_1, Φ and φ_2. In this study, it was assumed that the GBs had random misorientations that did not exceed 12°. GB regions were assumed to have a uniform width of 0.10 of the grain dimension.

A representative aggregate size was determined by modelling the response of aggregates with different numbers of grains (20, 30, 50 and 100 grains). Based on the convergence of the overall stress–strain response, it was determined that 50 grains would be sufficiently representative of material behaviour for a specimen

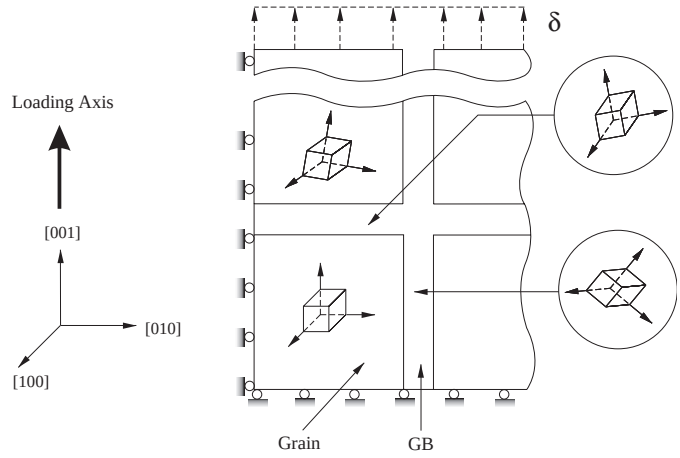

Figure 3. Polycrystalline and random crystallographic orientations.

with dimensions of 5 mm by 10 mm. This aggregate was subjected to an axial strain rate of $10^{-3}\,s^{-1}$ by applying a displacement along the [001] direction as shown in figure 3 for plane strain deformations. Symmetry boundary conditions were applied as shown in figure 3. Based on a convergence analysis, a minimum of 1915 four-node quadrilateral elements were used for the different analyses for this study.

The initial mobile dislocation density of the grain bulk was chosen as $10^{7}\,m^{-2}$, and the initial immobile dislocation density was chosen as $10^{10}\,m^{-2}$. In the interfacial GB regions, the initial mobile and immobile dislocation densities were varied as a function of the random GB misorientation (Ashmawi and Zikry 2002). Furthermore, it was assumed that the initial GB static yield stress is three times the grain bulk yield stress, and that the GB dislocations are of the same type as the bulk lattice. Using the method outlined by Kameda and Zikry (1996), the initial coefficient values, needed for the evolution of the immobile and mobile densities given by equations (6) and (7) were obtained as

$$g_{\text{minter}} = 5.53, \quad g_{\text{recov}} = 6.67, \quad g_{\text{immob}} = 0.0127, \quad g_{\text{sour}} = 2.7 \times 10^{-5}, \quad \frac{H}{K} = 3.289 \times 10^{3}\,\text{K}. \tag{21}$$

Different arrangements and combinations of void pairs were used, such that the effects of void interactions and growth could be realistically investigated (figure 4). Each void was chosen as circular with a radius of 0.01 mm, and each void was placed in the middle of a host grain. Three void distributions were chosen: a horizontal distribution of two voids (case 1), a vertical void distribution (case 2) and an inclined void distribution (case 3). Each distribution had two explicit voids (figure 4). The voids were initially distributed 0.11 mm apart for the vertical and horizontal distributions. For the inclined void distribution, the top void was oriented at 45° from the bottom void, and both voids were radially spaced apart by 0.156 mm. The results of this study will focus on how the interrelated effects of saturated dislocation densities on different slip systems, dislocation density transmission, impedance and blockage at GB interfaces, and void size affects and controls failure initiation at different physical scales.

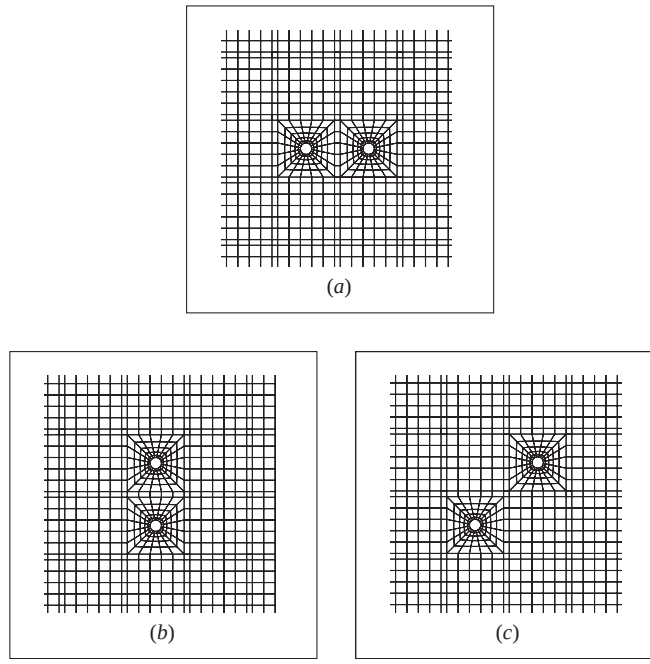

Figure 4. Two-void arrangements for: (*a*) case 1, (*b*) case 2 and (*c*) case 3.

7.1. *Saturated dislocation density effects*

The saturated mobile dislocation density for the most active slip systems, as a function of the nominal strain, is shown in figure 5. The mobile dislocation density saturation provides a measure of how the rate of inelastic activity, such as shear strain accumulation and porosity, occurs on different slip systems. Mobile densities corresponding to the rotated void arrangement (case 3) saturated to a maximum value at an earlier strain than the other two cases. Saturation for this case occurred at a nominal strain of 3.1% on the slip system $(11\bar{1})[\bar{1}0\bar{1}]$, compared with a nominal strain of 4.5% for case 1 (horizontal voids) for the slip system $(1\bar{1}1)[\bar{1}\bar{1}0]$, and with a nominal strain of 4.7% for case 2 (vertical voids) for the slip system $(1\bar{1}1)[\bar{1}\bar{1}0]$.

As can be seen from the contours for these mobile densities (figure 6), the maximum mobile densities have accumulated near the peripheries of the voids for case 3. For cases 1 and 2, there was no discernible mobile dislocation density accumulation at this nominal strain. Furthermore, as shown in figure 7, the accumulated plastic shear was 0.82 at a nominal strain of 3.1% for case 3 compared with 0.66 at a nominal strain of 4.5% for case 1 and 0.50 at a nominal strain of 4.7% for case 2. These accumulations for case 3 occurred near the void closest to the free surface. Furthermore, this void has deformed into an irregular elliptical shape. In these regions of accumulated plastic slip and mobile dislocation density, the porosity has attained limiting values. As shown in figure 8, the porosity for all three cases has attained an approximate value of 17%. However, the porosity distribution is markedly different for cases 1 and 2, compared with case 3. The maximum porosities occurred at the top for cases 1 and 2. For case 3, the maximum porosity occurred in the adjacent regions near the void. This indicates that microvoid nucleation and growth in terms of porosity f for this case, can lead to coalescence

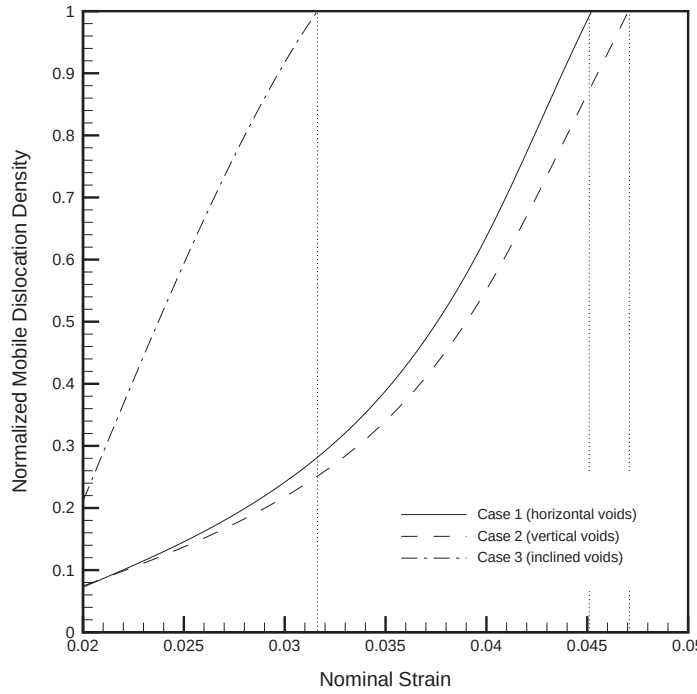

Figure 5. Normalized mobile dislocation density curves (most active slip systems) as a function of nominal strain.

between the two discrete voids. Hence, this increase in porosity accumulation is due to the void orientation along the maximum shear stress orientation of 45°. Furthermore, as seen from these contours, for cases 1 and 2, the porosities have accumulated near the free surface.

To ascertain the effects of the other active slip systems on void growth, coalescence and interaction, the evolution of the normalized mobile density as a function of the nominal strain was obtained (figure 9). As seen from this figure, the slip systems $(\bar{1}11)[\bar{1}\bar{1}0]$ and $(11\bar{1})[101]$ saturated at much lower strains of approximately 3.3% in comparison with the slip systems $(1\bar{1}1)[10\bar{1}]$ and $(11\bar{1})[011]$, which saturated at a nominal strain of approximately 7.5%. This may indicate that the slip systems that saturated at lower strains may be the operative slip systems that resulted in initial pile-ups at GB and in the ligament region. These pile-ups may result in the activation of adjacent slip systems that could relieve these accumulated densities by transmission mechanisms. If the pile-ups are not relieved, then microvoid nucleation in these locations may occur. For the slip systems $(1\bar{1}1)[10\bar{1}]$ and $(11\bar{1})[011]$ that saturated at the larger strains, the dislocation densities were localized in bands, in the ligament region, which extended between the voids, where the plastic strains have accumulated (figures 10 and 11).

Furthermore, as the global stress strain curve indicates, the stresses unloaded at approximately 5.1% (figure 12). This is the nominal strain at which the slip system $(111)[\bar{1}01]$ saturated (figure 9). This further indicates that global instabilities are directly linked to the *saturation* of different slip systems. As shown in figure 12, maximum porosities of 17% occurred in the regions of maximum mobile dislocation density near the loading surface and adjacent to the point of necking.

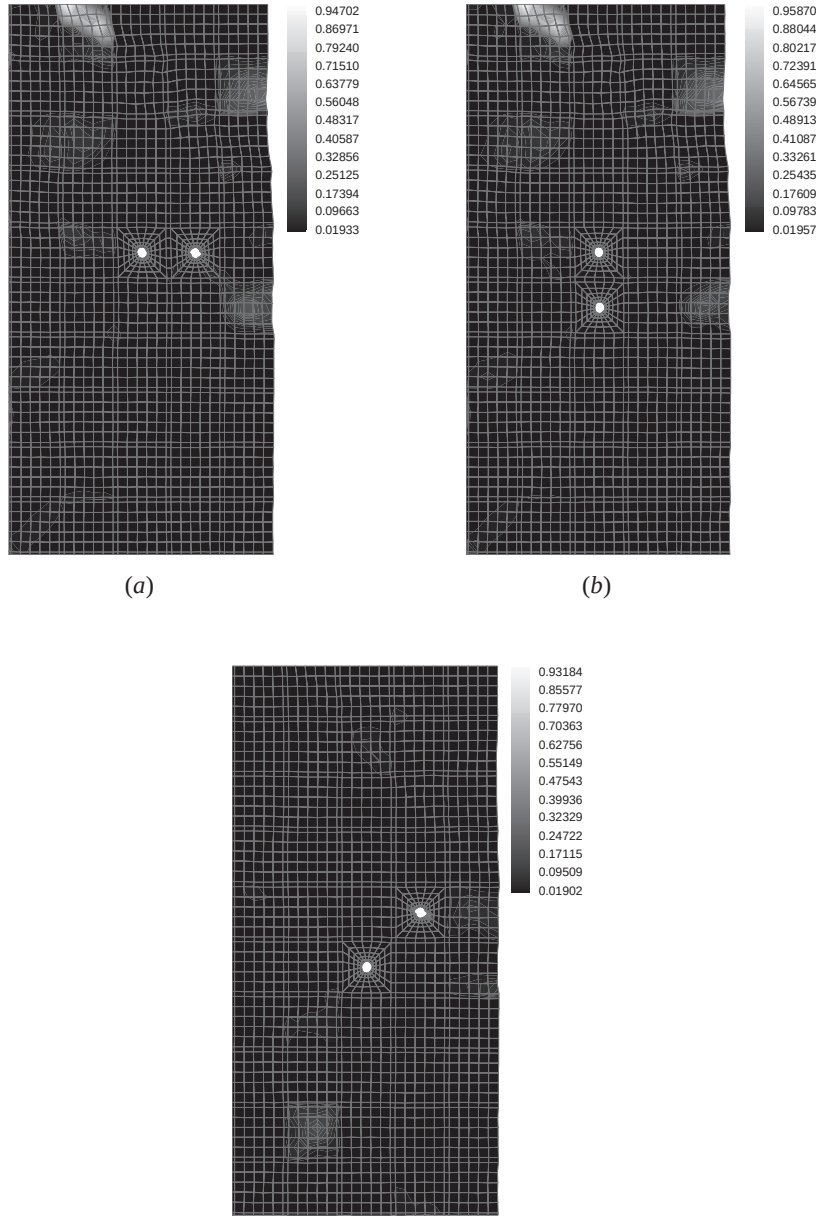

Figure 6. Normalized mobile dislocation densities on the slip systems (*a*) $(1\bar{1}1)[\bar{1}\bar{1}0]$ at 4.5% nominal strain, (*b*) $(1\bar{1}1)[\bar{1}\bar{1}0]$ at 4.7% nominal strain and (*c*) $(11\bar{1})[\bar{1}0\bar{1}]$ at 3.1% nominal strain.

Hence, mobile dislocation density evolution, saturation and interactions with GB interfaces play a major role in how dislocation density pile-ups and transmission affect and control void nucleation, growth and coalescence. To emphasize further this essential point, the transmission, impedance and blockage of different slip

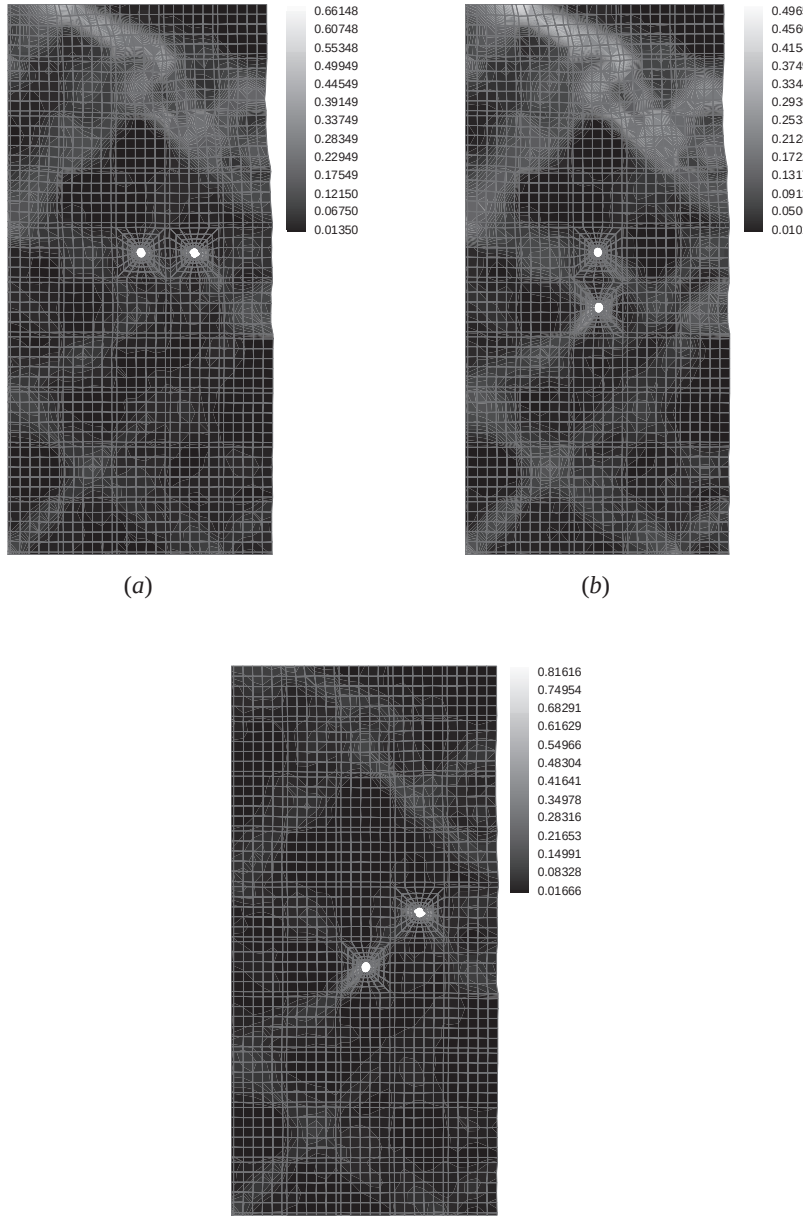

Figure 7. Accumulated plastic shear strains at (*a*) 4.5% nominal strain, (*b*) 4.7% nominal strain and (*c*) 3.1% nominal strain.

systems at different GB regions will be illustrated for the inclined void case in the next section.

7.2. *Grain-boundary transmission, impedance and blockage*

In figure 13(*a*), a potential dislocation density system, corresponding to the slip system $(11\bar{1})[011]$ at 5% nominal strain is shown for the inclined void case.

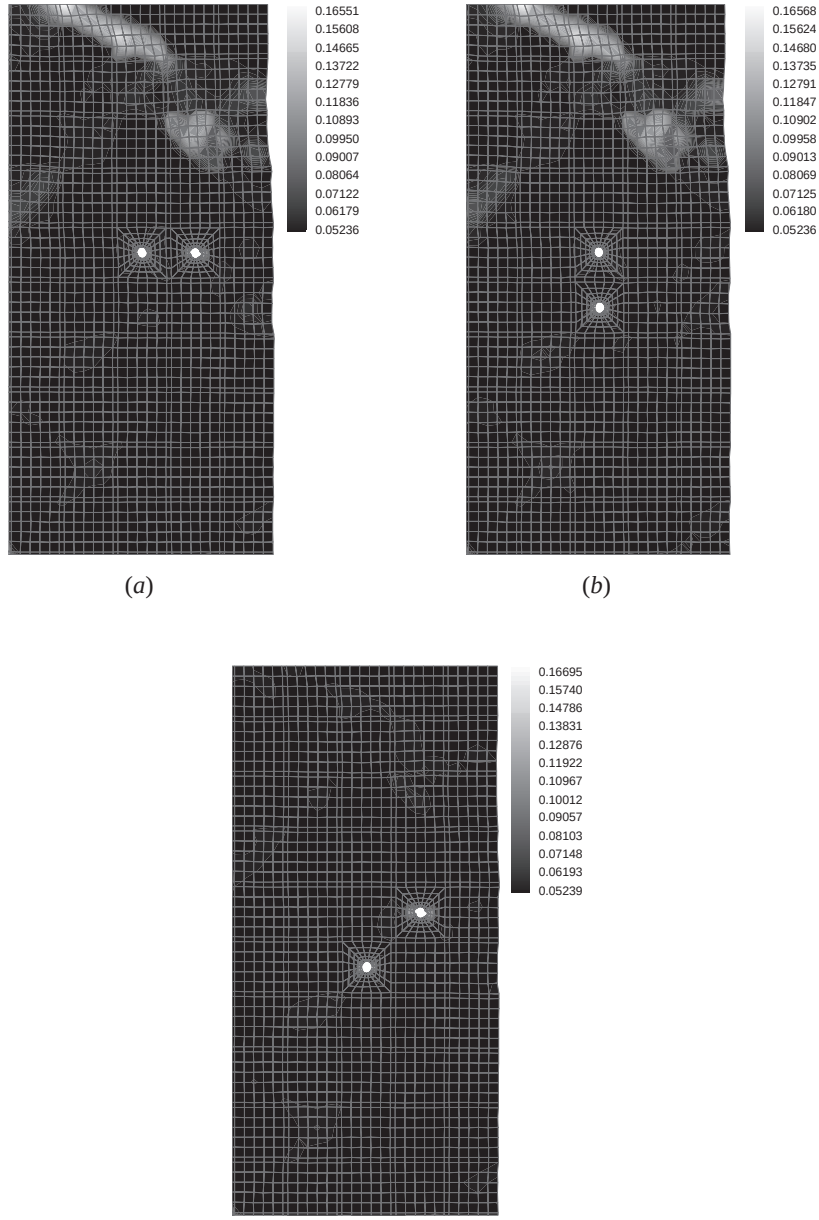

Figure 8. Porosity distributions at (*a*) 4.5% nominal strain, (*b*) 4.7% nominal strain and (*c*) 3.1% nominal strain.

As seen from this figure, potential dislocation density activities were localized in the ligament region, and at the top right-hand side of the aggregate. These regions are potential dislocation density regions that have been identified by the potential density envelope methodology outlined in §4. As the nominal strain increased to 8%, similar potential dislocation density activity sites can be activated (figure 13 (*b*)). Some of these potential activity sites might be relieved by transmitting the

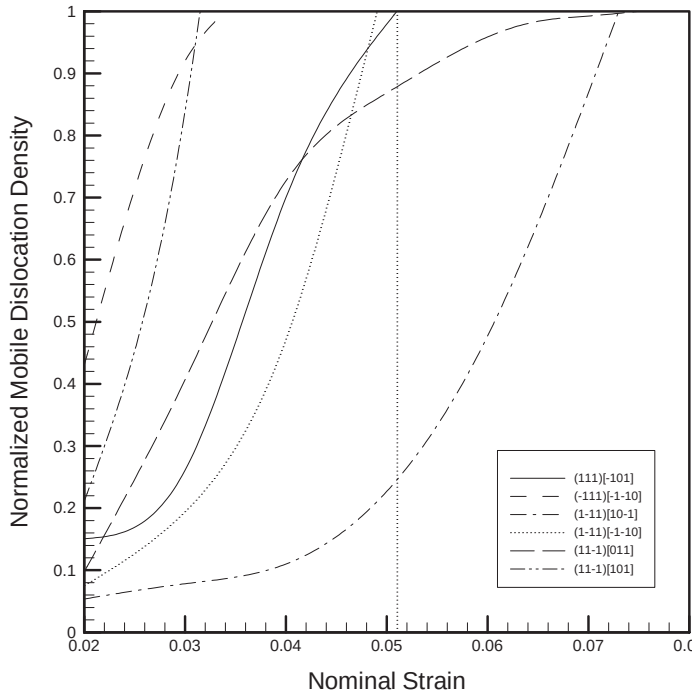

Figure 9. Most active saturated mobile dislocation density systems.

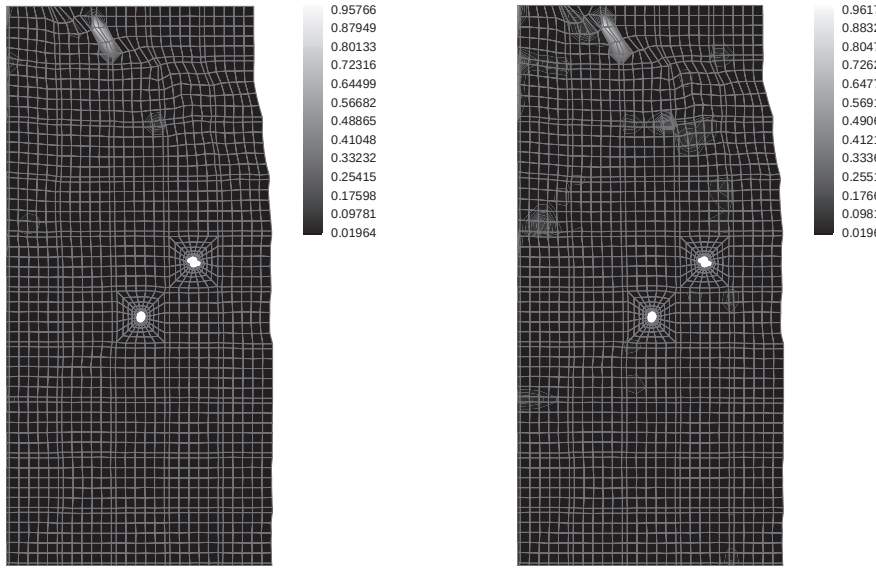

(*a*) (*b*)

Figure 10. (*a*) Normalized immobile dislocation density for the slip system $(1\bar{1}1)[10\bar{1}]$ at 7.3% nominal strain; (*b*) normalized mobile dislocation density for the slip system $(1\bar{1}1)[10\bar{1}]$ at 7.3% nominal strain.

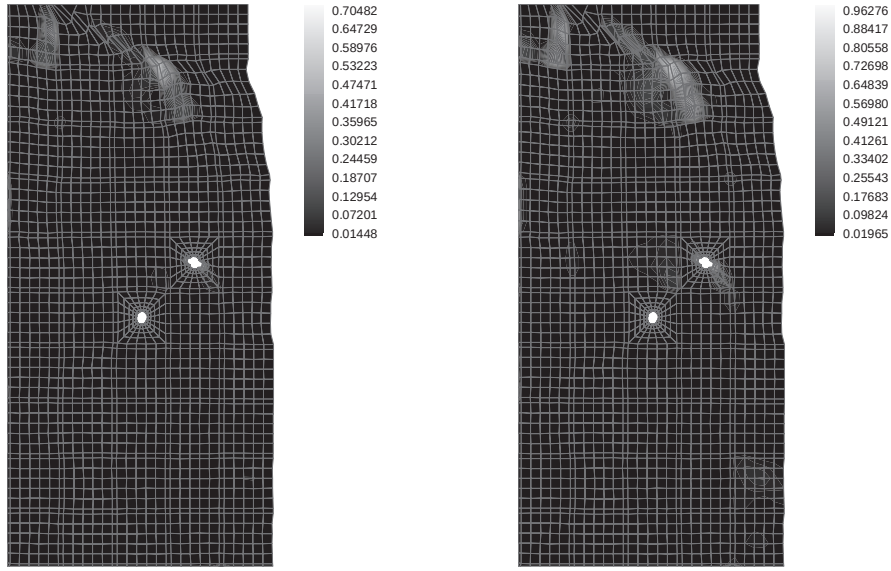

Figure 11. (*a*) Normalized immobile dislocation density for the slip system $(11\bar{1})[011]$ at 8% nominal strain; (*b*) normalized mobile dislocation density for the slip system $(11\bar{1})[011]$ at 8% nominal strain.

dislocation densities to the adjacent grains, or the dislocation densities might be absorbed by GBs, or the dislocation densities can accumulate near the GB regions and evolve into pile-ups.

In figure 14 (*a*), the cross-hatched area corresponds to a potential dislocation density activity site on the slip system $(111)[1\bar{1}0]$ at 8% nominal strain. In this case, using the dislocation-density–GB interaction scheme, 96% of the total dislocation density was transmitted through the GB, as shown in figure 14 (*b*), on the slip system $(11\bar{1})[1\bar{1}0]$. From the GB, the dislocation density was transmitted by the slip systems $(111)[01\bar{1}]$, $(111)[\bar{1}01]$ and $(111)[1\bar{1}0]$ to the adjacent grain (figures 14 (*c*) and (*d*)). Each of the slip systems transmitted one third of the total dislocation density emanating from the GB. Again the remaining residual (4%) of the total dislocation density in the grain could evolve to a potential site for dislocation density activities.

These transmission and blockage interactions at the GBs are occurring during the initiation and evolution of the different deformation and failure modes. These different interactions affect the evolution of porosity as the nominal strain changes. As seen in figure 15, the porosity distribution is affected by increases in the nominal strain. At lower strains, the maximum-porosity regions occurred near the void peripheries. However, as the strain increased to 8% nominal, the maximum porosity was concentrated not only in the ligament region between the voids but also in the region near the loading surface.

7.3. *Void size effects*

To investigate the effects of void size on failure initiation and failure, the top void size for the inclined void case (case 3) was increased by 100% to 0.02 mm.

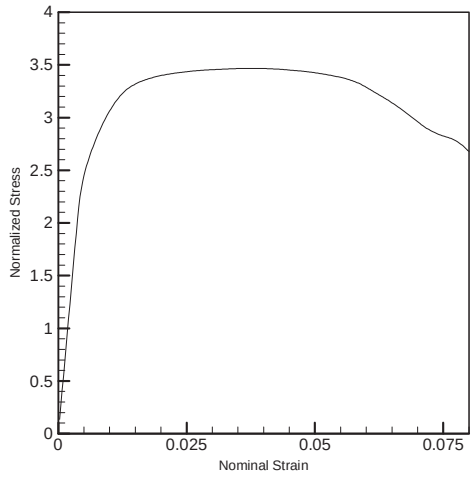

(*a*)

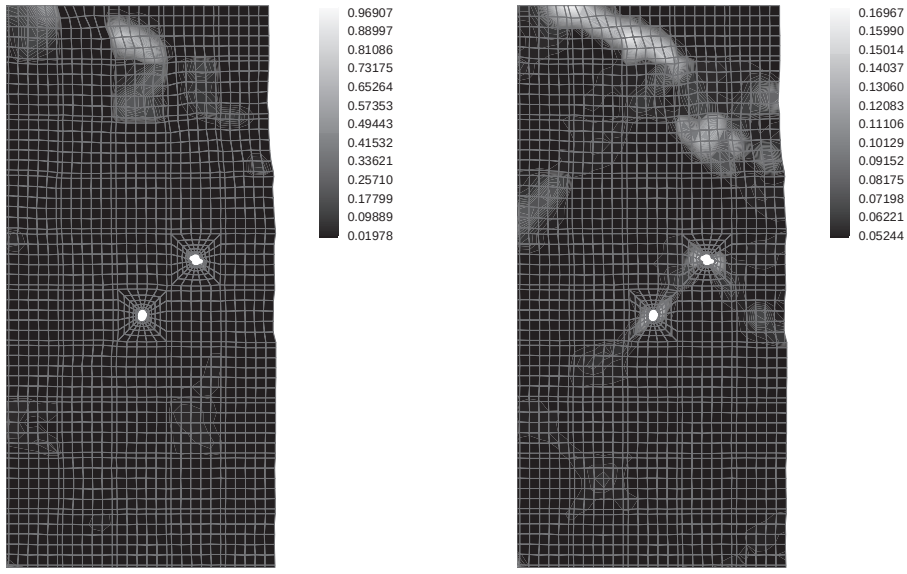

(*b*) (*c*)

Figure 12. (*a*) Global stress–strain curve for the inclined void case; (*b*) normalized mobile dislocation density for the slip system (111)[$\bar{1}$01] at 5.1% nominal strain; (*c*) porosity distribution at 5.1% nominal strain.

In figure 16, the normalized mobile dislocation density saturation curves are shown. As the nominal strain evolves to 8%, seven slip systems reached the saturation level. This was in contrast with the case with smaller voids (case 3), where only six systems attained saturation (figure 9). These slip systems, for the larger-void case, saturated faster as a function of nominal strain, in comparison with the smaller-void case.

The global stress–strain response for both this case and case 3 is shown in figure 17. The larger-void-size case unloaded at a much slower rate than case 3.

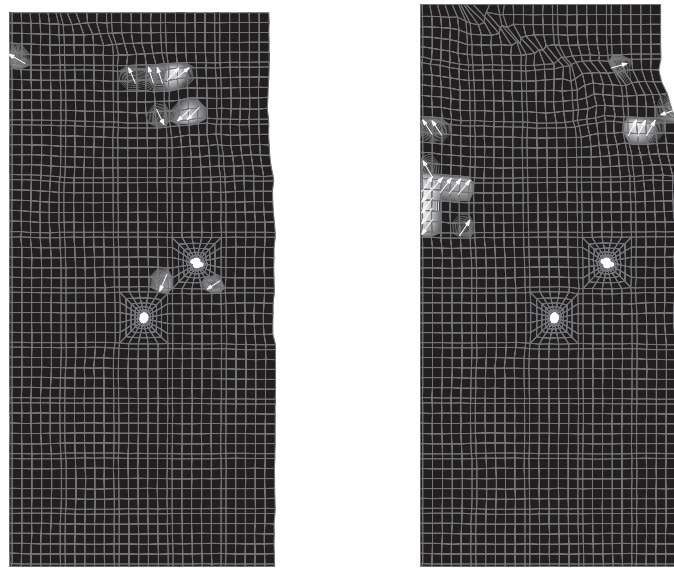

(*a*) (*b*)

Figure 13. Potential dislocation density activity sites at (*a*) 5% nominal strain for the slip system $(11\bar{1})[011]$ and (*b*) 8% nominal strain for the slip system$(\bar{1}11)[101]$.

This difference in behaviour is due to the interaction of the different dislocation density systems with the GB interfacial regions. In figure 18, the potential dislocation density activity sites corresponding to nominal strain of 8% are shown. These figures uniformly indicated that the majority of the transmission and pile-up activities occurred in the ligament, and near the larger void. These interactions resulted in a porosity evolution pattern far different from that for case 3, as shown in figure 19. For the larger-void case, at a 5% nominal strain, these porosity distributions clearly indicated that void coalescence would occur along the ligament region owing to void growth and coalescence. However, for case 3, the maximum porosity occurred near the loading surface and at the necking region. This difference in evolution is related to the presence of the larger void, which resulted in different dislocation-density–GB interactions.

At a nominal strain of 8%, although the maximum porosity for both cases localized between the voids (figure 20), it was more intense for the case of larger voids. This concentration of porosity was in both the ligament and the necking regions. For the smaller voids (case 3), the porosity region near the loading surface was also localized in the necking region, and it attained values similar to those in the ligament region.

In figure 21, the maximum dislocation densities and the orientations of the slip systems corresponding to specific slip systems were used to delineate regions of maximum porosity at a nominal strain of 8%. These results emphasized that the aggregate with the larger void will fail by coalescence in the ligament region between the discrete voids. For the aggregate with the smaller voids, specimen necking will most probably lead to failure. This is consistent with the experimental observations of Edelson and Baldwin (1962) and Bourcier and Koss (1985) for void-sheet formation.

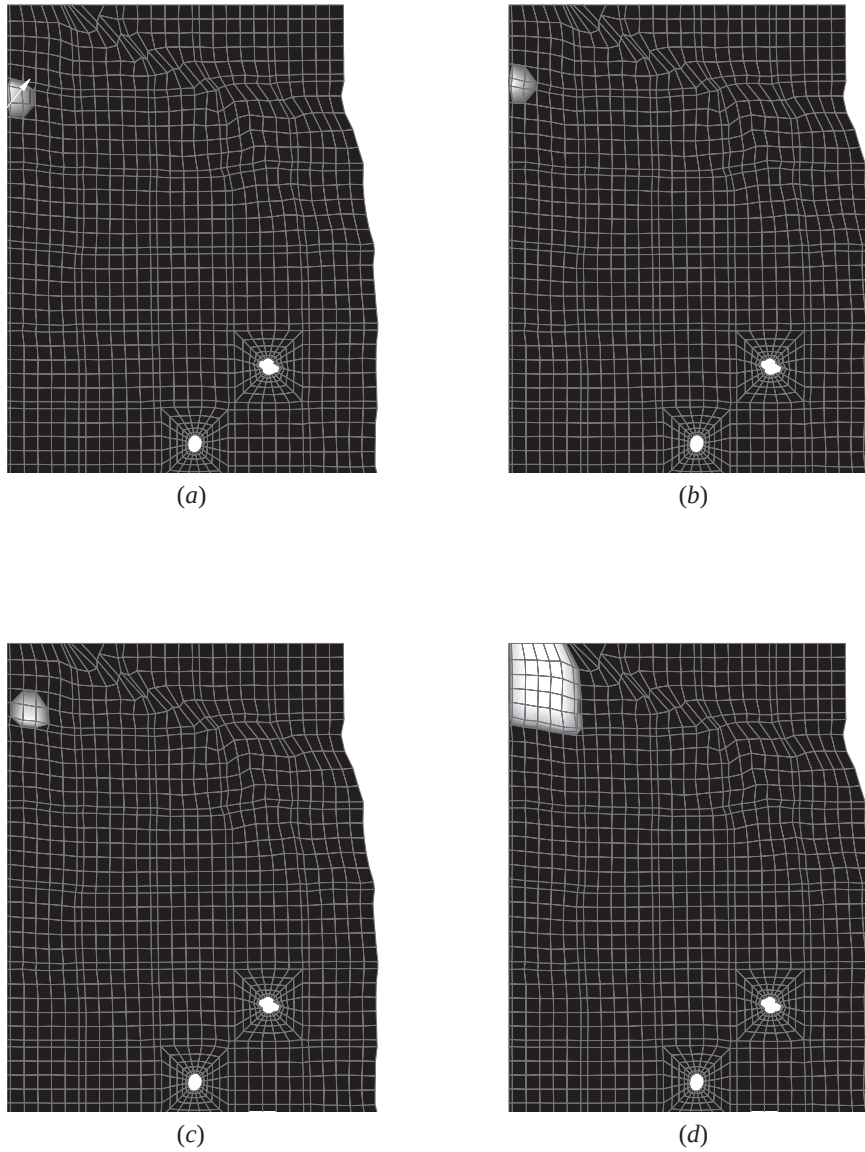

Figure 14. (*a*) Potential dislocation density activity site on the slip system $(111)[1\bar{1}0]$; (*b*) 96% transmission to a GB on the slip system $(11\bar{1})[1\bar{1}0]$; (*c*) full transmission from a GB to a neighbouring grain on the slip systems $(111)[01\bar{1}]$, $(111)[\bar{1}01]$, and $(111)[1\bar{1}0]$; (*d*) distribution within the neighbouring grain.

§8. Summary

This paper provides detailed predictive capabilities that have been used to understand complex interrelated multiscale physical mechanisms that result in void growth, interaction, coalescence and eventual ductile failure in porous fcc polycrystalline aggregates. A multiple-slip rate-dependent crystalline constitutive formulation that is coupled to the evolution of mobile and immobile dislocation densities, a new porosity formulation for microvoid nucleation and growth, and specialized

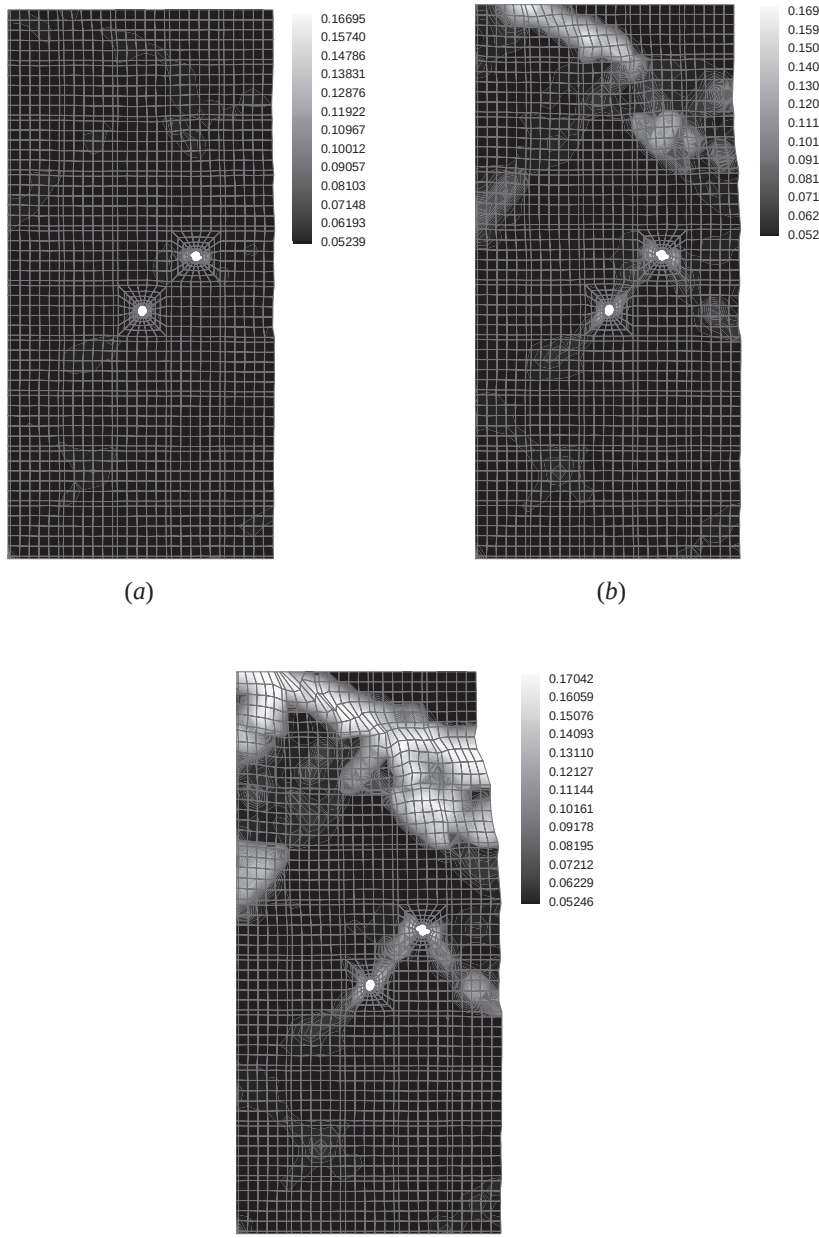

Figure 15. Porosity distribution at (*a*) 3.1% nominal strain, (*b*) 5.1% nominal strain and (*c*) 8.0% nominal strain.

computational schemes have been developed to investigate the effects of mobile and immobile dislocation densities, dislocation density transmission and impedance, and GB misorientation and structure on void growth, interaction and coalescence. GB interfacial kinematic conditions have been developed that account for a multitude of dislocation density interactions with GBs, such as full and partial

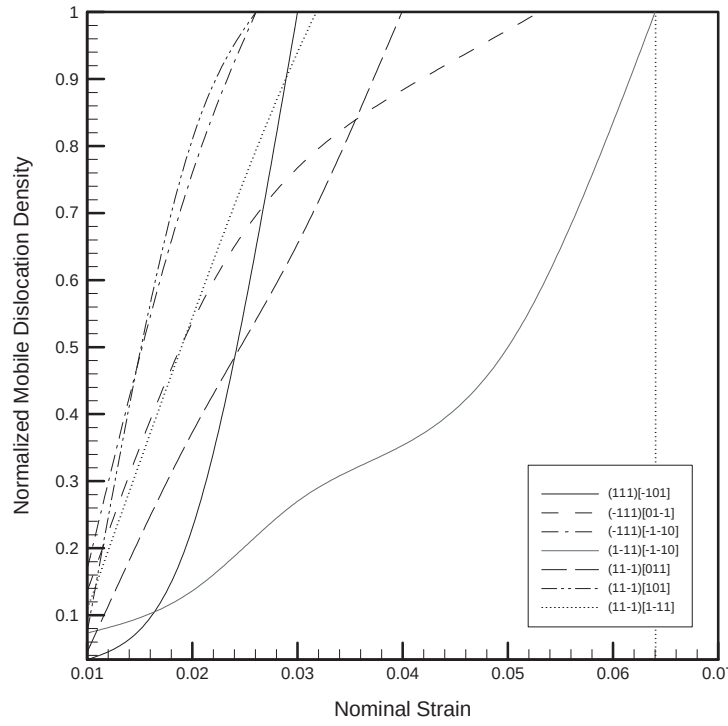

Figure 16. Saturation curves of the most active slip systems for the unequal-sized void case.

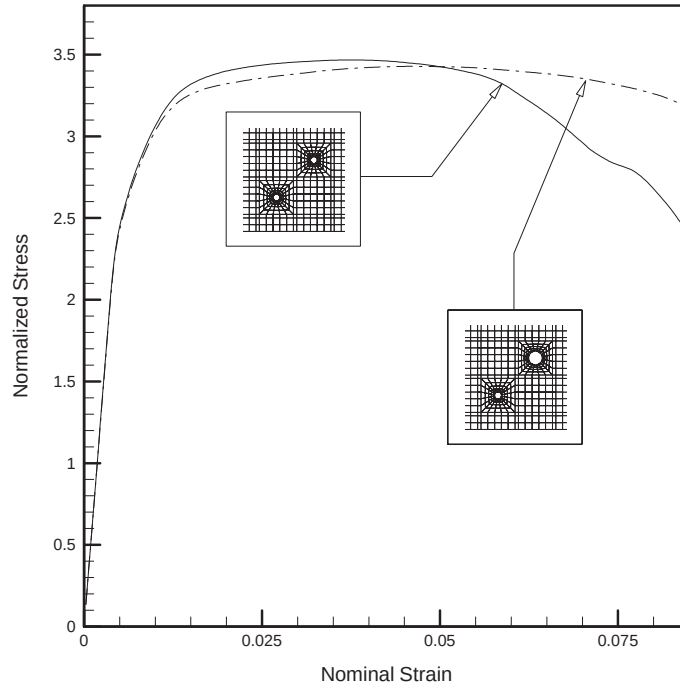

Figure 17. Global stress–strain curve.

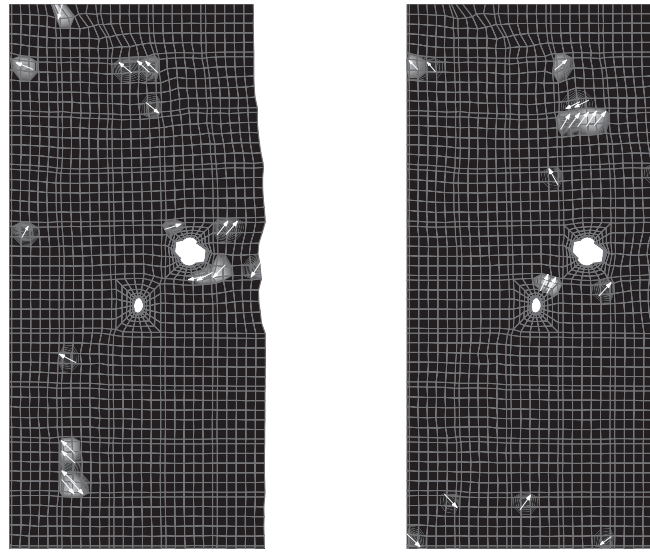

(*a*) (*b*)

Figure 18. Potential dislocation density activity sites at 8% nominal strain for (*a*) $(11\bar{1})[\bar{1}0\bar{1}]$ and (*b*) $(11\bar{1})[1\bar{1}0]$.

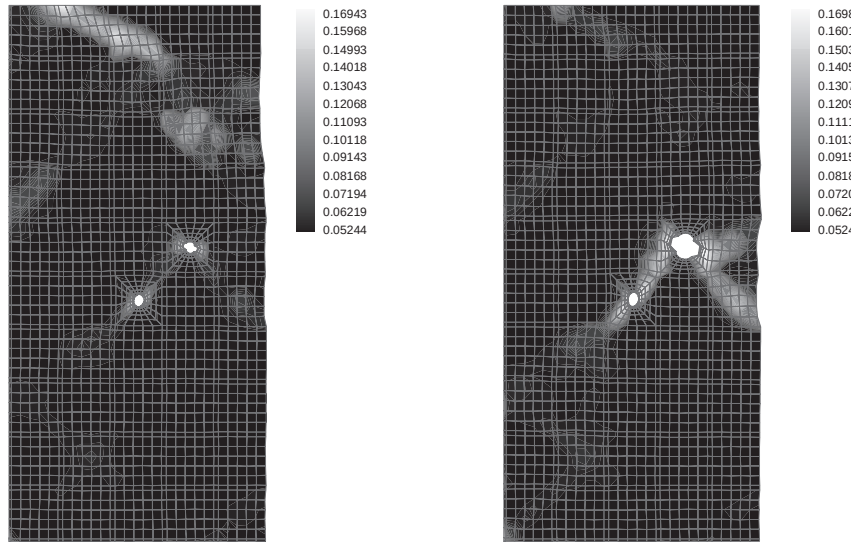

(*a*) (*b*)

Figure 19. Porosity distributions at 5.0% nominal strain for (*a*) the equal-sized void case and (*b*) unequal-sized void case.

transmission, impedance, blockage and absorption. This methodology can be used to identify and monitor pile-up and transmission regions as *deformation and failure modes initiate and evolve* pertaining to the different physical hierarchical scales associated with dislocation density evolution, GB structure and orientation, and void nucleation, growth and interaction.

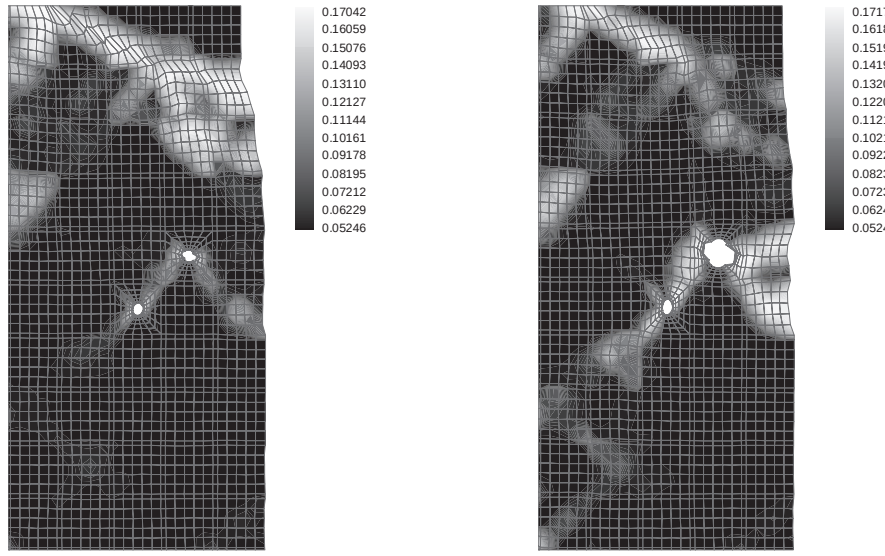

(*a*) (*b*)

Figure 20. Porosity distributions at 8.0% nominal strain for (*a*) the equal-sized void case and (*b*) unequal-sized void case.

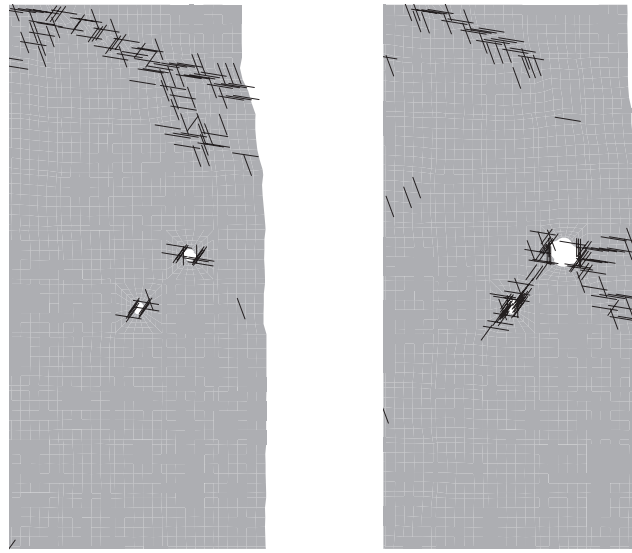

(*a*) (*b*)

Figure 21. Failure traces at 8.0% nominal strain for (*a*) the equal-sized void case and (*b*) unequal-sized void case.

For aggregates with different void pair arrangements, it was shown that mobile dislocation density evolution and its saturation on different slip systems and its interaction with GB interfaces play a major role in how dislocation density pile-ups and transmission affect and control void nucleation, growth and coalescence.

When the mobile dislocation density saturates on a specific slip system, this provides sites for localized interactions between explicit voids and substantial increases and localization of porosity and accumulated plastic strain. However, the mobile dislocation density saturation may also lead to GB blockage or absorption within the GB region. This can occur because there may not be preferentially oriented slip systems in adjoining grains to relieve a build-up of the accumulated dislocation density activities in the GB regions.

Analyses were also conducted to determine how changes in void pair sizes and spacing affected void-to-void interactions, and how this was related to dislocation density interactions with GB interfaces. It was shown that, as the void pair sizes were increased, the porosity, the stresses and the accumulated plastic strains were localized in the ligament region between the voids. This occurred because there was a significant number of regions for potential dislocation density activities as indicated by the saturation of the mobile dislocation densities of different slip systems in the ligament region. As the void size was decreased, there were fewer saturated slip systems and activities in the ligament region. There were also higher local stresses associated with smaller voids. The stresses are higher for the smaller void sizes, because of the build-up of dislocation densities at the GBs and around the void peripheries, which eventually leads to the global unloading of the stress. Therefore, there are two different types of failure associated with void pair size. As the void size is increased for different void pairs, porosity and interaction are localized in the ligament region. As void size is decreased, failure is due to the global unloading of the stress as a result of build-up of local stresses adjacent to the void peripheries.

Acknowledgements

This work was supported by Army Research Office grant DAAD19-02-1-0308, under the monitoring of Program Manager, Dr Bruce Lamattina. The computations were performed at the North Carolina Supercomputing Center (NCSC). The assistance of the staff at NCSC is deeply appreciated.

References

Ashmawi, W. M., and Zikry, M. A., 2000, *J. Comput.-Aided Mater. Des.*, **7**, 55; 2002, *J. Engng Mater. Technol.*, **124**, 88; 2003, *Mater. Sci. Engng*, **A343**, 126.

Baker, I., and Liu, F., 1994, *Mater. Res. Soc. Symp. Proc.*, **319**, 203.

Baker, I., Schulson, E. M., and Horton, J. A., 1987, *Acta metall.*, **35**, 1533.

Bay, B., Hansen, N., Hughes, D. A., and Kuhlmann-Wilsdorf, D., 1992, *Acta metall. mater.*, **40**, 205.

Becker, R., and Smelser, R. E., 1994, *J. Mech. Phys. Solids*, **42**, 773.

Bourcier, R. J., and Koss, D. A., 1985, *Adv. Fracture Res.*, **1**, 186.

Davies, P., and Randle, V., 2001, *Mater. Sci. Technol.*, **17**, 615.

Dingley, D. J., and Pond, R. C., 1979, *Acta metall.*, **27**, 667.

Edelson, B. I., and Baldwin, W. M. Jr, 1962, *Trans. Am. Soc. Metals*, **55**, 230.

Garrison, W. M., and Moody, N. R., 1987, *J. Phys. Chem. Solids*, **48**, 1035.

Gleiter, H., 1982, *Mater. Sci. Engng*, **52**, 91.

Hansen, N., 1990, *Mater. Sci. Technol.*, **6**, 1039.

Kameda, T., and Zikry, M. A., 1996, *Scripta mater.*, **38**, 631.

Kroner, E., 1986, *The Statistical Basis of Polycrystal Plasticity—Large Deformation of Solids*, edited by J. Gittus, J. Zarka and S. Nemat-Nasser (Amsterdam: Elsevier), pp. 27–39.

Lee, T. C., Robertson, I. M., and Birnbaum, H. K., 1990, *Metall. Trans.*, **21**, 2437; 1992, *Acta Metall. mater.*, **40**, 2569.

Liu, Q., Jensen, D. J., and Hansen, N., 1998, *Acta mater*., **46**, 5819.
Magnusen, P. E., Dubensky, E. M., and Koss, D. A., 1988, *Acta metall*., **36**, 1503.
Marguiles, L., Winther, G., and Poulsen, H. F., 2001, *Science*, **291**, 2392.
Mughrabi, H., 1987, *Mater. Sci. Engng*, **85**, 15.
Needleman, A., 1989, *Theoretical and Applied Mechanics*, Proceeding of a IUTAM Symposium, edited by P. Germain, M. Piau and D. Caillerie (Amsterdam: Elsevier Science Publishers), pp. 217–240.
Randle, V., 1997, *Acta mater*., **46**, 1459.
Schmitz, H. A., Dew-Hughes, D., and Bilello, J. C., 1989, *J. Mater. Res*., **4**, 1182.
Shen, Z., Wagoner, R. H., and Clark, W. A. T., 1988, *Acta metall*., **36**, 3231.
Watanabe, T., 1989, *Mater. Sci. Forum*, **46**, 25.
Watanabe, T., and Tsurekawa, S., 1999, *Acta mater*., **47**, 4171.
Werner, E., and Prantl, W., 1990, *Acta metall. mater*., **38**, 3231.
Zikry, M. A., 1994a, *Comput. Struct*., 337; 1994b, *Mech. Mater*., **17**, 273.
Zikry, M. A., and Kao, M., 1996, *J. Mech. Phys. Solids*, **44**, 1765.